Results in Physics 19 (2020) 103372

Contents lists available at ScienceDirect

Results in Physics

journal homepage: www.elsevier.com/locate/rinp

# Asymmetrical D-channel photonic crystal fiber-based plasmonic sensor using the wavelength interrogation and lower birefringence peak method

M. Ifaz Ahmad Isti[a,1], Hriteshwar Talukder[a,1], S.M. Riazul Islam[b,1], Samiha Nuzhat[a], A.S.M. Sanwar Hosen[c], Gi Hwan Cho[c,*], Shovasis Kumar Biswas[d,*]

[a] Department of Electrical and Electronic Engineering, Shahjalal University of Science & Technology, Sylhet 3114, Bangladesh
[b] Department of Computer Science and Engineering, Sejong University, Seoul 05006, Republic of Korea
[c] Division of Computer Science and Engineering, Jeonbuk National University, Jeonju 54896, South Korea
[d] Department of Electrical and Electronic Engineering, Independent University, Bangladesh (IUB), Dhaka 1229, Bangladesh

ARTICLE INFO

*Keywords:*
Asymmetry
Birefringence
Lower peak
Orthogonal polarization mode
Wavelength sensitivity

ABSTRACT

In this paper, an asymmetric photonic crystal fiber (PCF) working on surface plasmon resonance (SPR) has been proposed and demonstrated using the wavelength interrogation method and lower birefringence peak method. The proposed sensor contains a D-shaped analyte channel that can detect unknown analytes within the sensing range of 1.42–1.47 refractive index units (RIU) of the analytes. The structural asymmetry induces orthogonal x and y polarization modes. The numerical investigations with the finite element method (FEM) reveal that the sensor has a maximum wavelength sensitivity of 80,000 nm/RIU with a sensor resolution of $1.25 \times 10^{-6}$ RIU for the y polarization mode and the maximum figure of merit (FOM) is found to be of 370.4 $RIU^{-1}$. For the x polarization mode, the sensor exhibits a maximum wavelength sensitivity of 53,000 nm/RIU with a resolution of $1.89 \times 10^{-6}$ RIU, having a maximum figure of merit (FOM) of 351 $RIU^{-1}$. These results are found by using the wavelength interrogation method via confinement loss. On the other hand, the lower birefringence peak method-based analysis reveals a maximum wavelength sensitivity of 50,000 nm/RIU with a resolution of $2 \times 10^{-6}$ RIU. As such, it is highly suitable for organic chemical detections and medical diagnostics. In addition, this paper studies the fabrication tolerance on the sensor performance.

## Introduction

Surface Plasmon Resonance, an emergent technology, has presented unprecedented and eclectic progress in the realm of sensors due to its multifarious applications in the fields of bioimaging [1], chemical sensing [2] and environmental monitoring [3]. The application of SPR not only encompasses biomolecular analyte detection, but also conducts analysis as a label-free real time technology [4]. Despite the availability of other sensing mechanisms like intensity modulated sensors, wavelength modulated sensors, phase modulated sensors and polarization modulated sensors, SPR sensors stand out to be the most effective in terms of their superior sensing readings [5]. Surface plasmon resonance sensors have demonstrated exuberant and assorted capabilities over other sensing technologies like micro resonator, fiber bragg grating, multimode interference and resonant mirror through their elective and meticulous sensing tactic along with efficient light regulation. Previously, SPR sensors based on prism technology like slot waveguide and v- groove waveguide have been regarded as bulky and expensive. These impediments ultimately sculpted the way for PCF based SPR sensors as they substantiated qualities like portability, lightness in weight and remote detection skills. For SPR sensing applications, various configurations like micro fluidic slot based structures, long period fiber Bragg grating, D shaped structure, external and internal metal coated fibers have been extensively studied. Furthermore, the development of photonic crystal fibers has emerged steadily with their superior light confining capabilities, providing versatile applications in broadband optical communications as well [6]. The flexibility in the design of periodic arrangement of airholes in PCFs gives freedom to produce core guided optical modes, in accordance to the work demand. The present research works are focusing on the application of the physics of SPR on PCFs to produce enhanced results for analyte sensing purposes.

* Corresponding authors.
*E-mail addresses:* ifazst3@gmail.com (M.I.A. Isti), hriteshwar-eee@sust.edu (H. Talukder), riaz@sejong.ac.kr (S.M.R. Islam), samihanuzhat02@gmail.com (S. Nuzhat), sanwar@jbnu.ac.kr (A.S.M.S. Hosen), ghcho@jbnu.ac.kr (G.H. Cho), biswassk@iub.edu.bd (S.K. Biswas).
[1] These authors contributed equally to this work and co-first authors.

https://doi.org/10.1016/j.rinp.2020.103372
Received 7 July 2020; Received in revised form 19 August 2020; Accepted 28 August 2020
Available online 03 September 2020

Surface plasmon waves (SPW) occur at metal-dielectric interfaces, first demonstrated in 1957 [7], with Zenneck's contribution to theoretical introduction to SPR, coming in at 1907 [8]. Kretschmann [9] and Otto configurations [10] demonstrate the prism coupling mechanism to induce SPRs in metal dielectrics which are essentially utilized for detecting unknown refractive index of analytes. However, due to the bulky nature, its remote sensing applications are pretty limited. Hence, at present, SPR based PCF sensors are preferred due to its miniaturized size, design flexibility and enhanced sensing performance. The two groups of SPR PCF sensors are basically internally coated and externally coated sensors depending on the location of analytes and metal coating. The internal sensing technique offers higher sensitivity as the analyte directly alters the refractive index configuration of the fiber [11]. As SPR occurs at metal-dielectric interface, not all metals are suitable for supporting the optical phenomenon. Gold and silver are the most desirable choices as they are noble metals, showing inter-band transitions. Gold shows larger resonance peak shifts and is more chemically stable than most other metals [12]. Usage of silver points to a sharper resonance peak, but its formation of brittle oxide in aqueous environment restricts its practical applications [5]. The scientific communities and researchers have come up with versatile design structures with satisfactory sensing capabilities. A PCF SPR sensor has shown a wavelength sensitivity, $S_{\lambda=}$7040 nm/RIU with a sensing range of 1.40–1.42 [13]. Another PCF shows $S_{\lambda=}$4000 nm/RIU, with sensor resolution, $R = 2.5 \times 10^{-5}$ RIU [14]. A large D-shaped microfluidic channel based sensor has achieved a maximum $S_{\lambda=}$11,000 nm/RIU [15]. These investigations have been carried out, based on wavelength interrogation utilizing the confinement loss scheme. However, using the most recently developed lower birefringence peak method, a PCF sensor revealed $S_{\lambda=}$6,300 nm/RIU with R as low as$1.587 \times 10^{-5}$ RIU with a large sensing range of 1–1.43 [16]. The lower birefringence peak method is not dependent on the confinement loss of sensors, rather on the real part of the effective index of orthogonal core modes in asymmetric structures.

This work proposes an SPR based PCF sensor having a comparatively large microfluidic D-shape analyte channel with semi-hexagonal lattice of airholes. Gold has been chosen as the plasmonic metal. The D-channel hole causes the asymmetric core buildup of the structure, which induces the two orthogonal x and y polarization modes. The novel feature of this work is the study of both the confinement loss-based wavelength interrogation method and the lower birefringence peak method on a plasmonic sensor having a semicircular gold layer with an analyte filled D-channel. Considering the confinement loss scheme and carrying out the wavelength interrogation method, the x-polarization mode portrays a maximum $S_\lambda$ = 53,000 nm/RIU with a maximum FOM of 351$RIU^{-1}$ along with an $R = 1.89 \times 10^{-6}$ RIU. The y-polarization core guided mode shows a maximum $S_\lambda$ = 80,000 nm/RIU with a maximum FOM of 370.4 $RIU^{-1}$ along with an $R = 1.25 \times 10^{-6}$ RIU. Considering the lower birefringence peak method, a maximum $S_\lambda$ = 50,000 nm/RIU is achieved, leading to a sensor resolution $R = 2 \times 10^{-6}$ RIU. Hence, the proposed sensor is highly suitable for biochemical analyte detections as the sensitivity of the sensor is high. This work also focuses on fabrication tolerance of the sensor performance.

## Theoretical considerations

Coherent delocalized electron oscillations occurring in a metal conductor are called surface plasmons. Due to electronic transportations, longitudinal oscillations occur in the conductor to generate the surface plasmons when an external field is applied. A metal-dielectric supports surface plasmon polaritons (SPP) under resonance conditions, where SPWs propagate along the interface, which has a propagation constant [17]

$$\beta = \frac{\omega}{c}\sqrt{\frac{\epsilon_M \epsilon_D}{\epsilon_M + \epsilon_D}} \quad (1)$$

Here, $\omega$ is the angular frequency. c is the velocity of light. $\epsilon_M$ and $\epsilon_D$ are the permittivity of the metal and dielectric medium respectively.

Phase matching condition is ensured when the phases of SPWs and the applied EM field are matched along with their propagation constants coinciding with one another. Optical confinement because of photonic bandgap or modified total internal reflection (TIR) is the light guiding mechanism occurring in PCFs. Resonance takes place at the phase matching condition, where the frequency and the momentum of SPWs and incoming EM field coincide. Such phenomenon causes maximum modal power transfer from core guided mode to spp mode. When measured, the confinement loss takes the form of a gaussian shape because of its leaky gaussian core guided mode. The gaussian loss peak appears at the resonant wavelength, λ. This confinement loss is dependent on the imaginary part of the effective mode index [18]

$$CL = 8.686 \times k_0 \times Im(n_{eff}) \times 10^4 (dB/cm) \quad (2)$$

where, $k_0 = \frac{2\pi}{\lambda}$ is the wave number in vacuum and Im($n_{eff}$) denotes the imaginary part of the effective mode index. The wavelength interrogation method is solely dependent on the confinement loss, particularly, the imaginary part of the effective index. On the contrary, carrying out the sensor performance analysis via the lower birefringence peak method, lower peak of the birefringence curve corresponds to the resonating wavelength. Birefringence is observed for structural fibers presented with asymmetric cores. In metallized PCF, the differences of the real parts of the effective indices of x and y polarization modes represent birefringence [19]

$$B = Re_{eff}^{x} - Re_{eff}^{y} \quad (3)$$

where, $Re_{eff}^{x}$ and $Re_{eff}^{y}$ are the real parts of the effective indices of x and y polarization modes.

## Modelling and numerical analysis

The proposed sensor design consists of a semi-hexagonal 3-ring orientation of airholes with diameter, da. The airholes are arranged in this fashion so that the distance between consecutive airholes, i.e, the pitch, Λ is kept at 1.90 μm. The airhole da is related to the pitch by, da = 0.5Λ. The geometry of the proposed design contains a semicircular metal layer over silica, along with a D-channel, where the analyte needs to be introduced which is shown in Fig. 1(a). The working range of the sensor is between 1.42 and 1.47 of the refractive indices of analyte. For the corresponding wavelength ranges of the analyte index, the difference of the refractive index of silica and analyte induces photonic bandgap between analyte and silica. This causes the light confinement in the core region. Moreover, as there are no airholes in between the semicircular metallic layer and core region, guided mode is formed where the analyte has been introduced. Hence, evanescent waves can easily interact with metal surface electrons to produce surface plasmon waves (SPW). This causes the sensor to be highly sensitive to analyte changes.

Chemically stable gold is chosen as the plasmonic metal with thickness, tg = 40 nm. Gold with thickness below 10 nm is impractical as it forms discontinuous film [20]. Our proposed sensor has a gold layer which is much higher than the practical limit to avoid fabrication impediments. The micro-fluidic D-channel (MFC) needs the introduction of analytes within it. Stack and draw method is a practical way of introducing circular airholes [21]. The D-MFC can be subjected to modified chemical vapor deposition (CVD) preform with flat ground at a side [22]. To precisely formulate the residual diameter, rough edges are polished for fabricating D-shaped preform [23]. CVD also allows gold layer deposition with minimized surface roughness. For uniform coating, atomic layer deposition (ALD) is another alternative for the metal layer deposition [24]. A metal layer can be deposited using

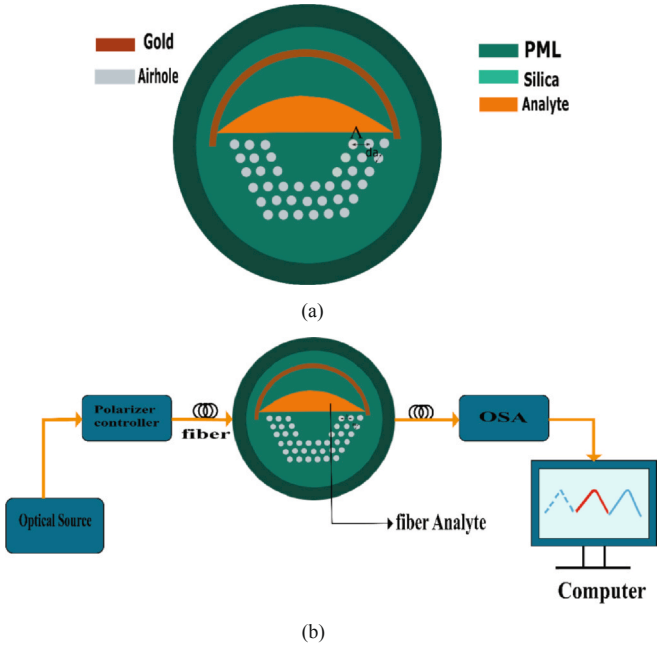


**Fig. 1.** (a) Geometry and (b) Experimental setup of the proposed design.

thermal evaporation, pulsed laser deposition (PLD) or electron beam deposition (EBD) through nanosphere masks [25]. Nanosphere lithography (NSL) efficiently produces nanoparticle arrays with controlled size and shape. The localized SPR (LSPR) peak shift studies have been conducted using the NSL as the fabrication technique for metal layer formation along the dielectric in [25]. The effect of silica overlayer thickness variations have also been studied in the LSPR shifts.

An optical source can pass light through a polarizer controller into the fiber, which is spliced with the PCF SPR sensor (Fig. 1(b)). The output is passed to an optical spectrum analyzer (OSA) to get the reading in a computer. Any change detected in analyte index is picked up by the sensor and subsequent resonant wavelength changes are detected by a spectrometer. Refractive index of the back ground material is chosen to be silica which is likely to be more insensitive to temperature, calculated via Sellmeier's equation [6]

$$\eta_{si}^2(\lambda) = 1 + \frac{B_1\lambda^2}{\lambda^2 - C_1} + \frac{B_2\lambda^2}{\lambda^2 - C_2} + \frac{B_3\lambda^2}{\lambda^2 - C_3} \tag{4}$$

where, $B_i$ and $C_i$ are sellmeier coefficients for silica where i = 1,2,3 with λ being the wavelength.

Plasmonic metal, gold has a dielectric function derived from the drude model [18]

$$\epsilon_d = \epsilon_\infty - \frac{\omega_D^2}{\omega(\omega + j\gamma D)} - \frac{\Delta \epsilon\, \Omega_L^2}{(\omega^2 - \Omega_L^2) + j\Gamma_L\omega} \tag{5}$$

in which, $\epsilon_\infty = 5.9673$ which is the permittivity at high frequency, $\omega_D$ and $\gamma_D$ are the plasma and damping frequencies respectively. The rest of the parameters have been taken from [18].

Finite element method (FEM) is the numerical tool with which simulation works have been carried out in comsol multi-physics software. A non-physical perfectly matched layer (PML) has been chosen as the boundary condition which acts as an absorber of radiation and reflected light at the boundary. Triangular mesh elements divide the entire geometry, where the maximum and minimum element sizes are $1.68 \times 10^{-6}$ m and $7.52 \times 10^{-9}$ m respectively, which ensures the propagation of wave. Maximum element growth rate is chosen to be 1.3, which allows element size to grow from smaller element regions to higher ones. Usually, letting this value be close to 1 is desirable. The ratio of the boundary element size to the curvature radius is 0.3. These give a strong simulation environment to have better accuracy in reaching solutions with the eigen value solver.

## Results analysis and discussion

### *Wavelength interrogation method*

Fig. 2 (a) and (b) portray the x and y polarized core modes forming the core of the guided mode. Fig. 2 (c) and (d) are the associated spp modes. The spp mode in Fig. 2 (c) couples itself to the x-polarized core mode and the spp mode in Fig. 2(d) couples itself to the y-polarized core mode. This results in maximum power transfer from the core guided light to the surface plasmonic waves (SPW) which leads to the resonance coupling between the core guided modes to the spp modes at the resonance wavelengths. This has been portrayed with the electric field profile in Fig. 2 (e) and (f). The real part of effective indices of the x and y polarization modes establish crossings with that of the associated spp modes. These crossings ensure the phase matching of the EM field and the SPWs. The central airholes are removed for the stability of core mode with respect to changes in λ. Fig. 3 elucidates the gaussian confinement loss of the two modes corresponding to their resonant wavelength, λ. For pragmatic implementation, a good sensing response for both the orthogonal modes provide more freedom in choosing the light source [18]. Our proposed sensor shows a good response for both modes. For the analyte refractive index change from 1.42 to 1.47, the gaussian peak and resonance λ shifting is portrayed in Fig. 4(a) and 5(a) for the x and y polarization modes.

The ideal structural parameters for the design are tg = 40 nm, Λ = 1.90 μm and da = 0.5Λ, found after several deliberate iterations performed in determining the optimized structure. An increase of refractive index of the analyte causes subsequent blue shifting of the gaussian peak, which can be detected by a spectrometer. Both orthogonal polarization modes show the same optical property.

Fig. 4(a) illustrates the shifting of the CL spectra with small increase of RI for x polarization mode. The confinement loss appears to increase with the increase of RI from 1.42 to 1.45 and the spectra indicates significant red shifting with decrease of RI. On the contrary, the CL spectra appears to decrease with the increase of RI from 1.45 to 1.47. Fig. 4(b), (c) and (d) illustrate the CL spectra in accordance with the subsequent changes in tg, Λ and da for the x polarization mode. With the increase of tg, confinement losses indicate trivial depreciation. A reduced amount of energy transfer is extrapolated from this, as thicker gold layer obstructs penetration of the evanescent field. By increment of Λ from 1.8 to 2 μm, a substantial amount of loss decreases, thereby demonstrating reduced interaction. There have been no observable shifts in variation of the pitch. The saturation of confinement loss can be articulated by varying the da from 0.4Λ to 0.5 Λ as depicted in Fig. 4(d) with no apparent shifting.

Fig. 5(a) portrays the behavior of the CL spectra with respect to the changes in RI in y polarization mode. For decline of the analyte index from 1.46 to 1.43, confinement loss decreases owing to reduced energy transfer from core to SPWs. However, at na = 1.42, the structure shows significant increase in confinement loss along with an increased red shift. Fig. 5-(b), (c) and (d) show an illustration of the CL spectra for y polarization mode. Increasing gold layer thickness causes blue shifting of the gaussian curve for both orthogonal modes and no definitive change in its loss. For alteration of the Λ from 1.8 to 2 μm, gaussian response is steeper at 1.90 μm but no wavelength shifting occurs. The fractional increase or decrease of the diameter of airholes has negligible effect on the sensor performance. The wavelength interrogation method reveals a sensor resolution [18]

$$S_\lambda[nm/RIU] = \frac{\Delta\lambda}{\Delta n_a} \tag{6}$$

where, $\Delta\lambda$ being the peak wavelength shifts and $\Delta n_a$ denoting to consecutive analyte index difference. Figure of merit (FOM) is a significant parameter to scrutinize the sensor's gaussian response. The FOM is

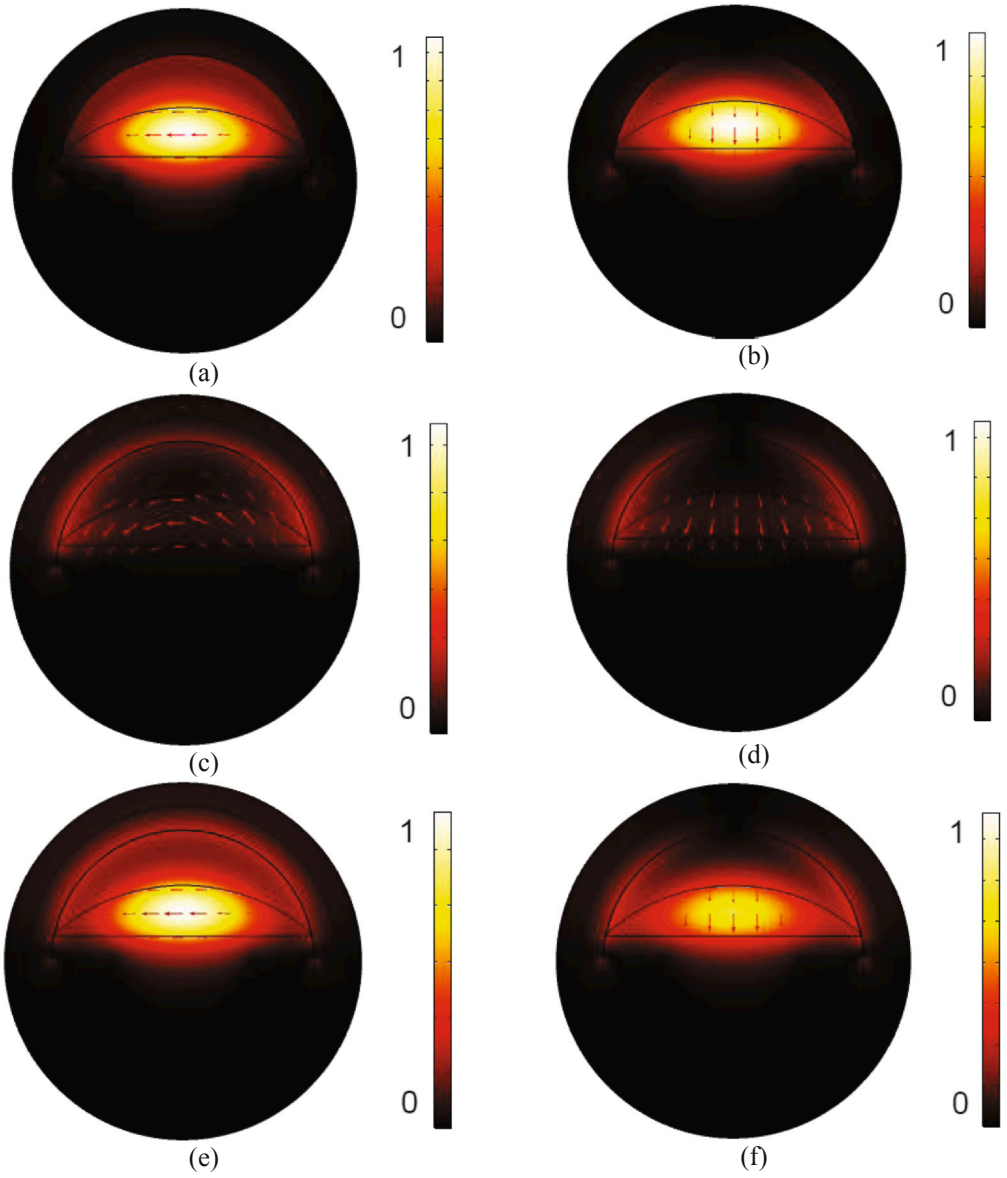


**Fig. 2.** Electric field distribution of the (a)‘ core mode (x-polarized) (b) core mode (y-polarized), (c) spp mode coupled to the x-polarized core mode (d) spp mode coupled to the y-polarized core mode (e) and (f) represents the resonance coupling of the spp modes with the orthogonal core modes.

inversely proportional to the full w idth half maximum (FWHM) of the gaussian loss curves [26]

$$FOM = \frac{S_\lambda}{FWHM} \tag{7}$$

Tables 1 and 2 uphold the sensor performance for the orthogonal polarization modes.

Maximum resonant λ shift occurs for $n_a = 1.45$ for x-pol mode and that for y-pol mode occurs at $n_a = 1.42$. The resonant shifts are considerable and appear to be uniformly distributed throughout the analyte RI. Within tabular data, a highest FOM of 351 $RIU^{-1}$ and 370.4 $RIU^{-1}$ are observed for the x-pol and y-pol mode respectively. Higher confinement loss is an impediment to the sensor design as it limits the sensor length causing hindrance in getting a viable and measurable output signal. The maximum propagation loss for x and y pol modes are 137 dB/cm and 97.1 dB/cm respectively.

The sensor wavelength resolution evaluates the sensor performance [18]

$$R = \Delta n_a \Delta\lambda_{min}/\Delta\lambda_{peak} RIU \tag{8}$$

where $\Delta\lambda_{min} = 0.1nm$ is considered as the minimum spectral resolution [18]. The sensor resolution is inversely proportional to wavelength sensitivity. The proposed sensor shows a minimum sensor resolution of $1.89 \times 10^{-6}$ RIU and $1.25 \times 10^{-6}$ RIU respectively.

*Lower birefringence peak method*

The lower birefringence peak method is carried out and studied for asymmetric PCF sensors. Unlike the confinement loss scheme, birefringence of a PCF is not dependent on the imaginary part of the effective mode index. As discussed in the theoretical analysis, it is solely dependent on real parts of the orthogonal modes induced into the structure because of asymmetric core modes. The birefringence curve of a metallized PCF sensor has an upper and a lower peak. The lower peak corresponds to the resonant λ and their difference is termed as resonance intensity [27]. In this scheme of analysis, changes in the analytes corresponding to their refractive indices, are successfully detected by changes in the resonant λ and resonance intensity.

Fig. 6 portrays the dispersion relations and their corresponding birefringence. The lower peak is denoting resonant wavelength. Fig. 7 (a)

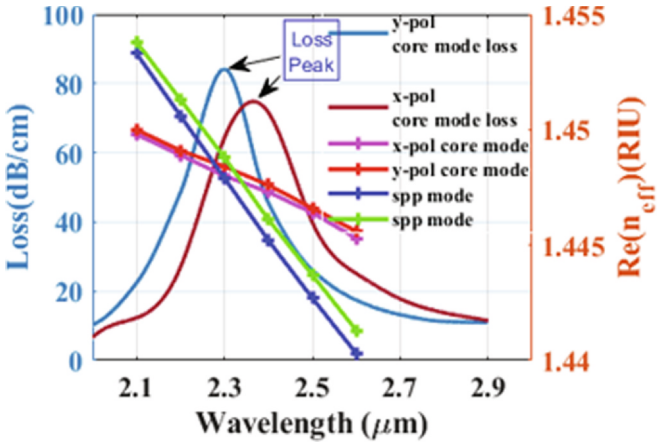


**Fig. 3.** Dispersion relations of the x-pol core mode (pink), y-pol core mode (red) and the spp modes (dark blue, green) with gaussian confinement loss, x-pol (brown) and y-pol (light blue) with parameters na = 1.46, tg = 40 nm, Λ = 1.90 μm, da = 0.5Λ. (For interpretation of the references to colour in this figure legend, the reader is referred to the web version of this article.)

shows that analyte index variations from 1.42 to 1.47 causes blue shifting of the birefringence curve. The shift in lower peak, picked up by a spectrometer, is the shift of the resonant λ. Furthermore, the analyte index changes have an effect on resonant intensity, it rises, followed by a subsequent decline. Fig. 7 (b), (c) and (d) come up with the fabrication tolerance on the birefringence curves. The increase of metal layer thickness causes the blue shifting of the birefringence curve, followed by a subsequent decrease of resonant intensity. Pitch variations have more impact on the resonant intensity. For the airhole da variations, increasing da to more than 0.5Λ, causes birefringence curve to shift upward. The lower peak in the birefringence curve representing the resonant λ is similar to the loss peak of the x-polarization mode obtained from the confinement loss method [16]. The shifting of the lower peak, detecting the analyte changes is related to the wavelength sensitivity, which evaluates the sensor performance [27]

$$S_\lambda[nm/RIU] = \frac{\Delta\lambda}{\Delta n_a} \tag{9}$$

where, $\Delta\lambda$ represents the lower peak shifts with respect to analyte index change $\Delta n_a$. Table 3 evaluates the sensor performance in terms of birefringence.

The highest $S_\lambda$ is observed for $n_a$ = 1.44, which is of 50,000 nm/RIU with a resolution as low as $2 \times 10^{-6}$ RIU.

*Comparative analysis*

Table 4 comes up with a comparative argument of the results of the proposed sensor in terms of the wavelength interrogation method via

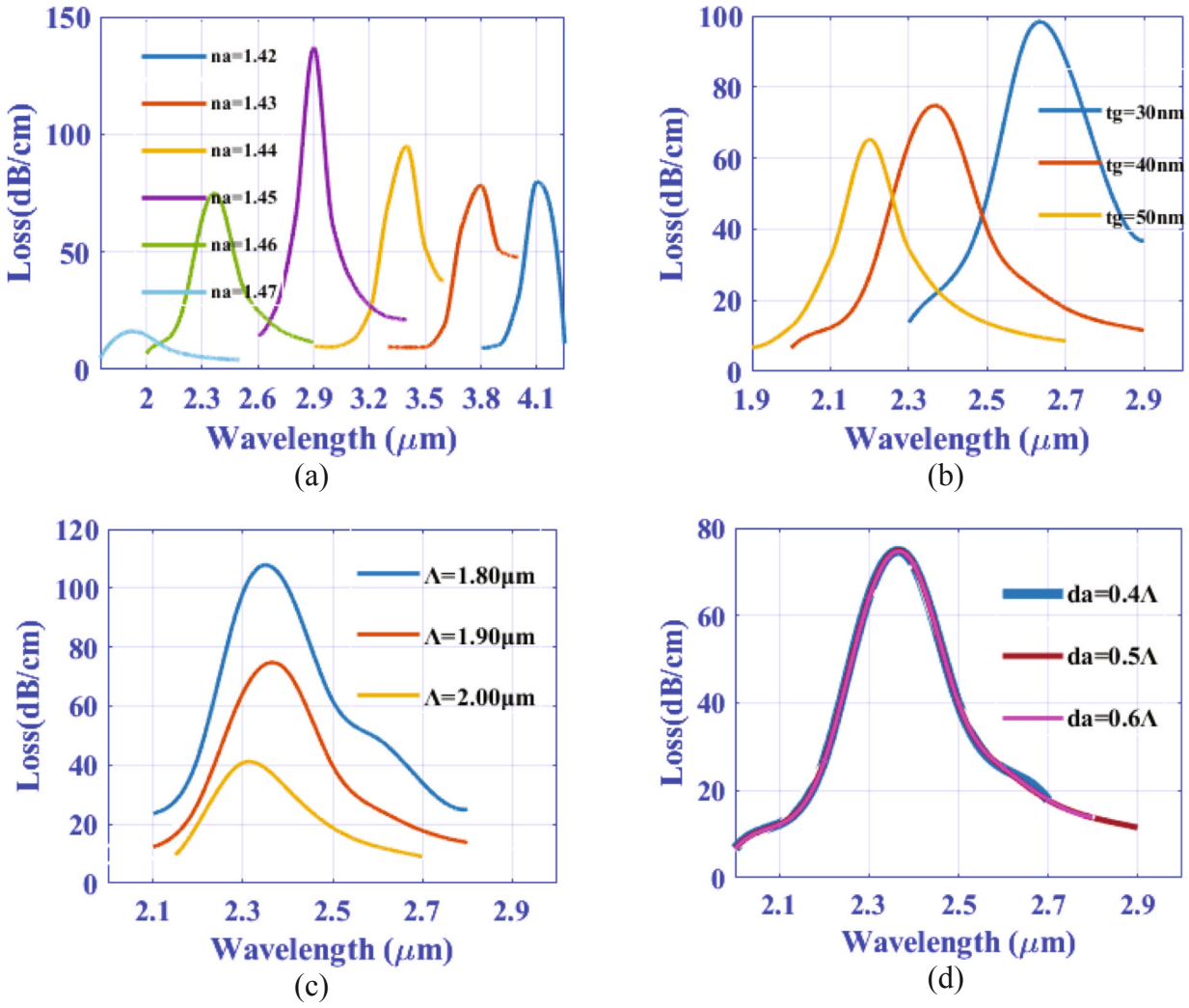


**Fig. 4.** Loss curves for x-polarization, with varying (a) analyte index (b) gold layer (c) pitch and (d) airhole diameter.

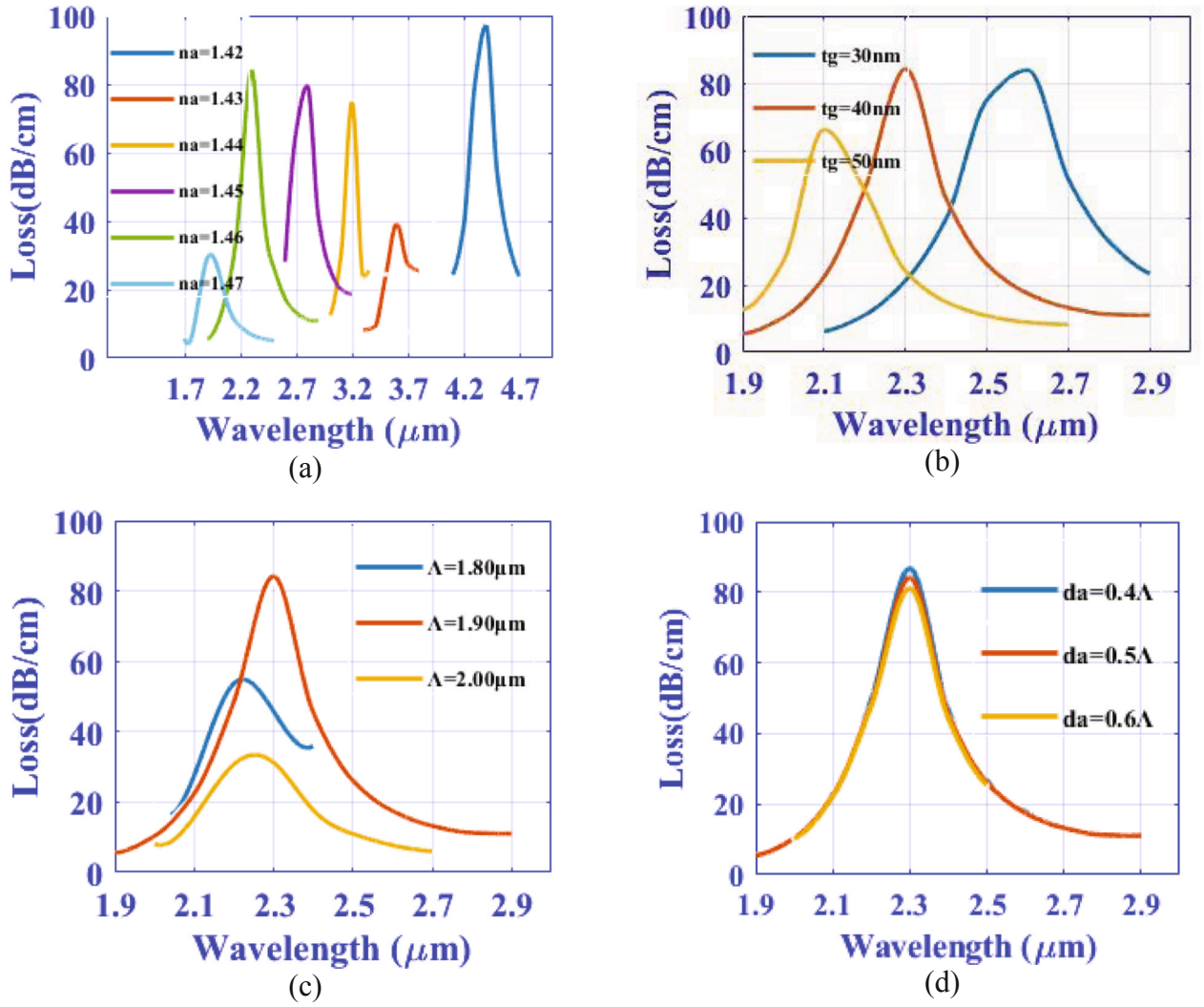


**Fig. 5.** Loss curves for y-polarization, with varying (a) analyte index (b) gold layer (c) pitch and (d) airhole diameter.

**Table 1**
Sensor performance within the sensing range for x-polarization.

| Analyte index | $\alpha_{peak}$ (dB/cm) | $\lambda_{peak}$ (μm) | FOM ($RIU^{-1}$) | $S_\lambda$ (nm/RIU) |
|---|---|---|---|---|
| 1.42 | 80 | 4.1 | 150.8 | 30,000 |
| 1.43 | 78.2 | 3.8 | 242.4 | 40,000 |
| 1.44 | 95 | 3.4 | 280.9 | 50,000 |
| 1.45 | 137 | 2.9 | 351 | 53,000 |
| 1.46 | 74.8 | 2.37 | 168.6 | 44,000 |
| 1.47 | 16.2 | 1.93 | N/A | N/A |

**Table 2**
Sensor performance within the sensing range for y-polarization.

| Analyte index | $\alpha_{peak}$ (dB/cm) | $\lambda_{peak}$ (μm) | FOM ($RIU^{-1}$) | $S_\lambda$ (nm/RIU) |
|---|---|---|---|---|
| 1.42 | 97.1 | 4.4 | 344.8 | 80,000 |
| 1.43 | 39.2 | 3.6 | 341.9 | 40,000 |
| 1.44 | 74.7 | 3.2 | 370.4 | 40,000 |
| 1.45 | 79.6 | 2.8 | 219.3 | 50,000 |
| 1.46 | 84.2 | 2.3 | 200 | 37,000 |
| 1.47 | 30.2 | 1.93 | N/A | N/A |

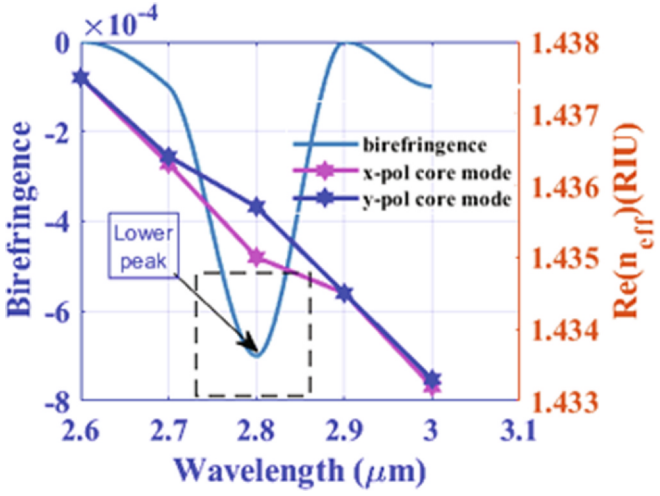


**Fig. 6.** Dispersion relations of the x and y polarization modes and their birefringence curve.

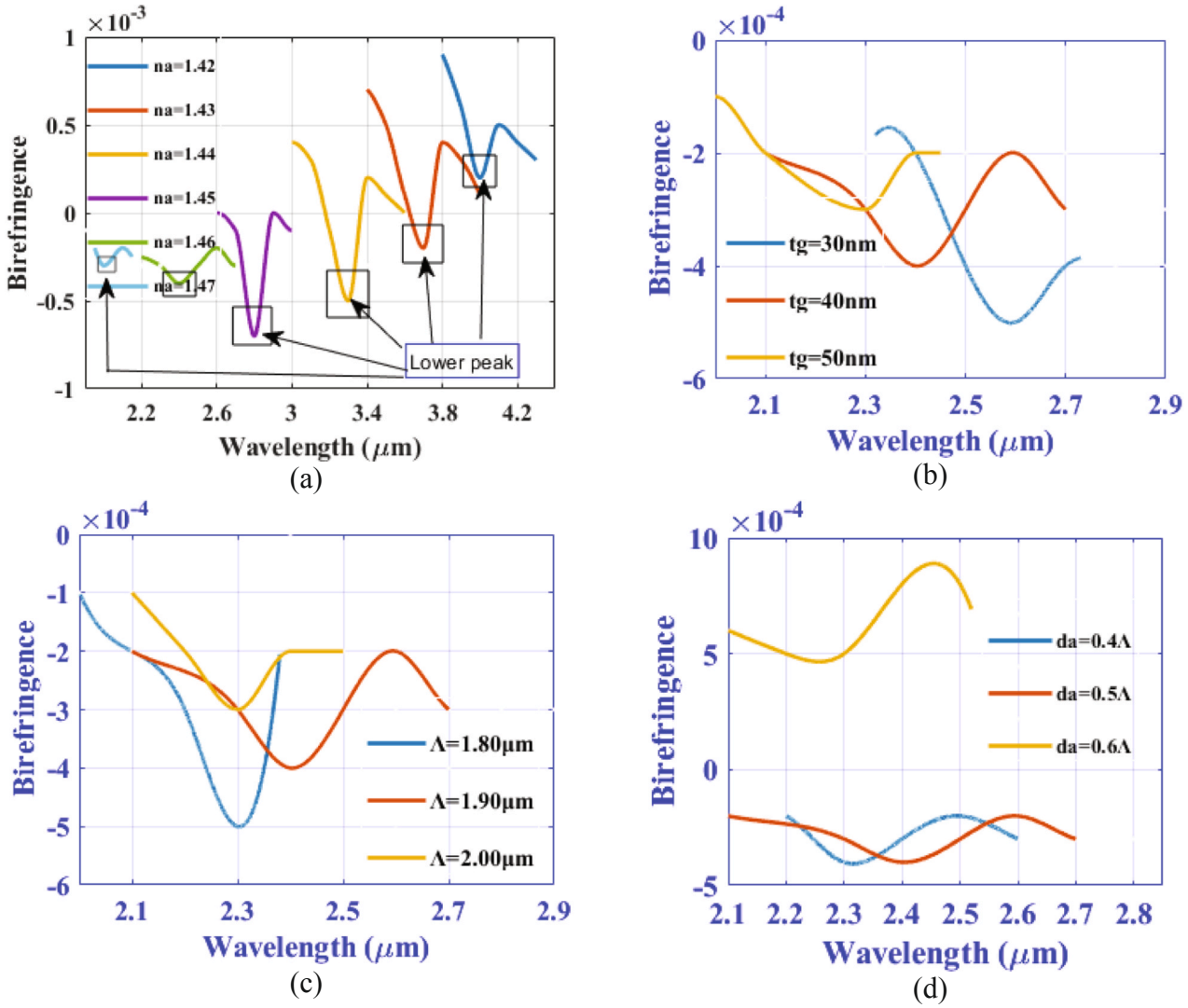


**Fig. 7.** Birefringence curve for the metallized PCF with (a) analyte index variation (b) gold layer thickness (c) pitch and (d) airhole diameter.

**Table 3**
sensor performance within the sensing range with birefringence peak shift studies.

| Analyte index | $\lambda_{peak}$ (μm) | Resonance Intensity | Resolution (RIU) | $S_\lambda$ (nm/RIU) |
|---|---|---|---|---|
| 1.42 | 4 | $2.995 \times 10^{-4}$ | $3.33 \times 10^{-6}$ | 30,000 |
| 1.43 | 3.7 | $5.998 \times 10^{-4}$ | $2.5 \times 10^{-6}$ | 40,000 |
| 1.44 | 3.3 | $6.998 \times 10^{-4}$ | $2 \times 10^{-6}$ | 50,000 |
| 1.45 | 2.8 | $6.999 \times 10^{-4}$ | $2.5 \times 10^{-6}$ | 40,000 |
| 1.46 | 2.4 | $1.998 \times 10^{-4}$ | $2.5 \times 10^{-6}$ | 40,000 |
| 1.47 | 2 | $9.95 \times 10^{-5}$ | N/A | N/A |

confinement loss scheme. The PCF SPR sensor shows a very high wavelength sensitivity in comparison to other recent works and the numerical value is the highest within the sensing range 1.42–1.47 to the best of our knowledge.

Table 5 draws out a comparative analysis with recent publications on PCF SPR sensors in terms of the lower birefringence peak method. To our best knowledge, carrying out analysis based on birefringence method, our proposed sensor surpasses other works in terms of wavelength sensitivity and minimum spectral resolution.

**Table 4**
Comparison of recent publications with respect to the confinement loss based wavelength interrogation.

| Ref. | Structure | WS (nm/RIU) | FOM ($RIU^{-1}$) | RI Index |
|---|---|---|---|---|
| [28] | D shaped | 46,000 | N/A | 1.33–1.43 |
| [29] | Circular lattice | 9000 | N/A | 1.34–1.37 |
| [30] | D-shaped | 31,000 | N/A | 1.32–1.4 |
| [18] | Scaled-down | 30,000 | 508 | 1.33–1.39 |
| [31] | Dual micro channel | 13,000 | N/A | 1.23–1.29 |
| [32] | D shaped | 20,000 | N/A | 1.18–1.36 |
| [33] | Au-$TiO_2$ based | 25,000 | 502 | 1.33–1.38 |
| [34] | H shaped | 25,900 | N/A | 1.33–1.49 |
| [35] | Circular slotted lattice | 16,000 | 400 | 1.4–1.46 |
| Proposed design (x-pol) | D-channel Semi-hexagonal | 53,000 | 351 | 1.42–1.47 |
| Proposed design (y-pol) | D-channel Semi-hexagonal | 80,000 | 370.4 | 1.42–1.47 |

*Sensor evaluation*

The sensor shows a very good linear fit for x and y polarization modes in terms of confinement loss scheme and also for birefringence

**Table 5**
Comparison of recent publications with respect to lower birefringence peak shifts.

| Ref. | Structure | WS (nm/RIU) | Resolution (RIU) | RI Index |
|---|---|---|---|---|
| [27] | Hexagonal lattice | 22,000 | $4.55 \times 10^{-6}$ | 1.33–1.42 |
| [19] | Circular lattice | 16,700 | $5.99 \times 10^{-6}$ | 1.33–1.42 |
| [16] | Square lattice | 6,300 | $1.587 \times 10^{-5}$ | 1–1.43 |
| Proposed design | D-channel Semi-hexagonal | 50,000 | $2 \times 10^{-6}$ | 1.42–1.47 |

curve shifting which is shown in Fig. 8. The governing characteristic curves for the x and y orthogonal modes and birefringence curve shifting are $y = -45x + 68$, $y = -48x + 72$ and $y = -41x + 62$ respectively. The analysis of the sensitivity performance of D-channel semi-hexagonal PCF SPR sensor reveals the sensor to be an ecclesiastical candidate for analyte sensing. Likewise, the fabrication tolerance is studied on the sensor characteristics, which shows a satisfactory result, making it a viable candidate for pragmatic implementations. The sensor is studied with both the confinement loss dependent wavelength interrogation method and the recently developed lower birefringence peak method and the results are compared. Both the analysis reveal the sensor performance to be satisfactory.

In this paper, we investigated and focused on the behavior of the structure around RI 1.42–1.47 owing to its possible real time application in chemical and environmental sensing. There are various chemical agents possessing the RI within the specified range from 1.42 to 1.47 (for example, polylactic acid = 1.46, glycerol = 1.4729, Carbon Tetrachloride = 1.46, 60% glucose solution in water = 1.4394).

These analyte RI alterations are the key to picking up sensor responses. The resonant wavelength shifts with the local RI change in the core region investigated via the wavelength interrogation technique, can be detected by the optical spectrum analyzer when the output is passed through it. Also, the lower peak birefringence method confirms the same. The spectrum is analyzed in a computer later on. Initially, the biosensor has to be spliced with fibers in the input and output of the sensor. It is suggested that single-mode fibers are spliced such that only the core guided modes are passed on to the sensor, eliminating the other radiation modes or lossy modes. The SPR biosensor shows a good sensing response in both the orthogonal modes. Hence, polarizing the light in specified planes is important initially before the incident light is

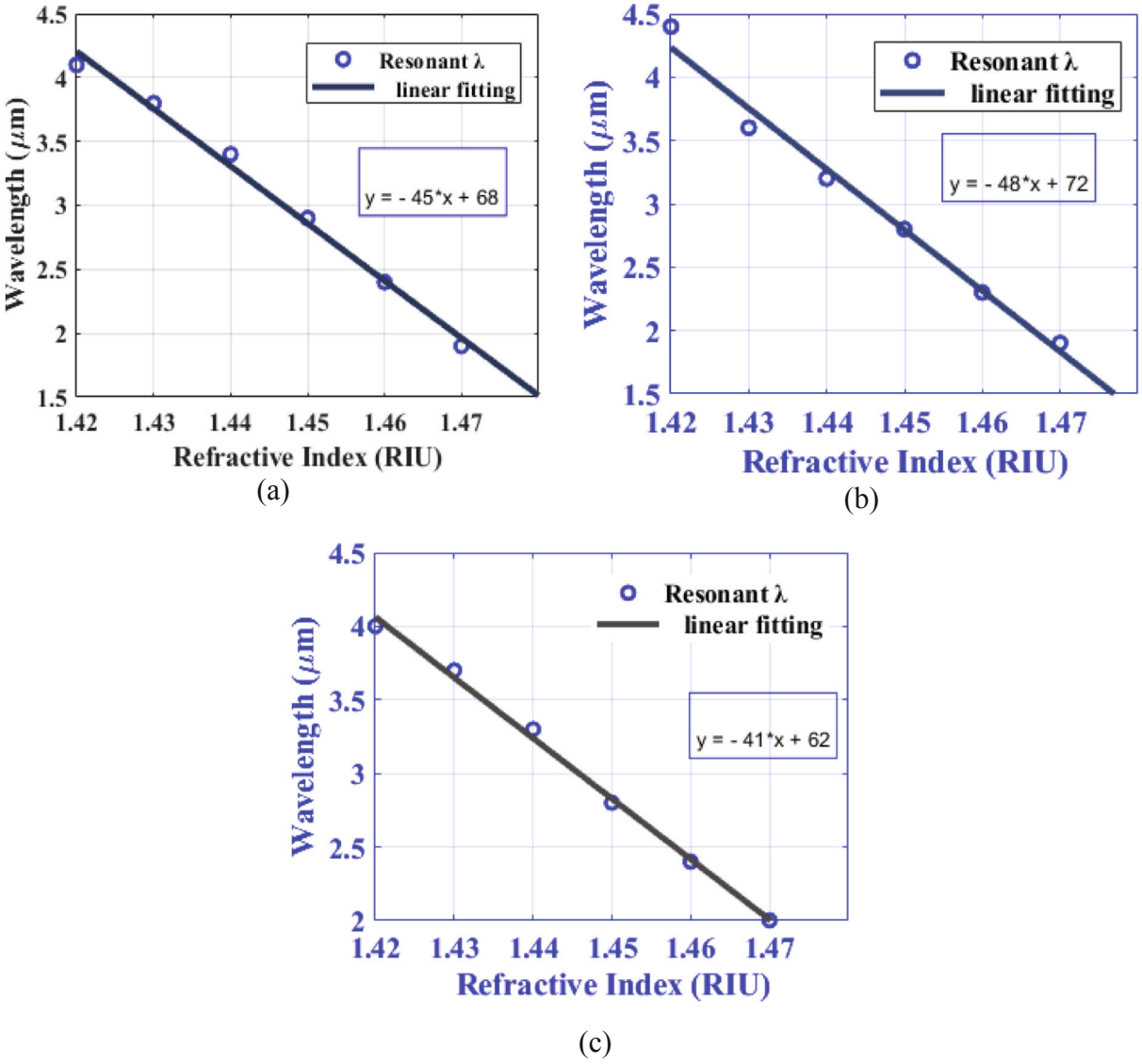


**Fig. 8.** Resonant λ versus analyte index changes for confinement loss method with (a) x-pol mode (b) y-pol mode and (c) with birefringence curve shifts.

made to enter the sensor.

*Practical prospect of analyte sensing*

SPR based sensing is remarkable when it comes to analyte sensing. The refractive index change of the analyte in close contact with the metallic nanoparticles causes sharp intensity changes in the output. These nanoparticles behave as transducers which convert the local RI to spectral shifts in the propagation loss. Recently, a research team has been able to come up with a plasmonic biosensor with experimental verification of Covid19 diagnosis using the PPT (Plasmonic Photothermal Effect) combined with localized SPR [36]. The binding events that occur cause the local analyte RI on the nanoparticles to change. This has been utilized for the genetic testing and the nucleic acid detection of the virus. This PPT based LSPR method provides a much more reliable, fast and precise alternative for Covid19 detection when compared to the presently used RT-PCR (Reverse Transcription Polymerase Chain Reaction) technique. It has been reported that localized SPR shifts have been previously used for measuring concentrations of a neurotoxin, Amyloid $\beta$-Derived Diffusible Ligand (ADDL), which plays a significant role in the progression of Alzheimer's Disease [37]. Generally, organic molecules have higher refractive indices which are suitable to be detected with our modeled sensor with high and sharp sensitivity. In Ref. [38], a majority portion of the refractive index of toluene, benzene, chloroform and carbon di-sulfide lies in the sensing region of our proposed sensor. Glucose is a relatively important organic compound, which is reasonable to represent blood components. Different concentrations of glucose solutions lie within the RI sensing range of 1.33–1.47 [39]. The sensing range of our proposed sensor falls a subset to this RI sensing range.

*Fiber limitations and further discussion*

The alteration in RI with temperature changes is defined by the thermo-optic coefficient ($\frac{dn}{dT}$) of any material. The $\frac{dn}{dT}$ of the waveguide silica is very small, which is $7.8 \times 10^{-6}$ per degree Celsius [40]. This suggests that the waveguide silica is almost insensitive to temperature changes, which makes it a suitable candidate for analyte sensing with PCFs [41]. However, the core region guides light through the analyte. Hence, the $\frac{dn}{dT}$ of the analyte has a greater impact on the effective mode index of the core mode. Any alterations in the effective index will cause the resonance wavelength to occur at slightly shifted wavelengths. It is suggested that the temperature remains steady and stable when the analyte is made to flow in the analyte channels of the sensor. In addition to this, splicing loss may occur when splicing the sensor to the fibers connected to the input and output of the PCF. The study of splicing losses is beyond the scope of numerical investigations of the PCF SPR sensors.

## Conclusion

In this work, an asymmetric SPR based PCF sensor is proposed which has a D-shaped MCF channel. Gold is used as a chemically stable plasmonic metal. The confinement loss-based wavelength interrogation method reveals the maximum wavelength sensitivity of the sensor to be 53,000 nm/RIU and 80,000 nm/RIU for x and y polarization modes, respectively along with a figure of merit (FOM) of 351 $RIU^{-1}$ and 370.4 $RIU^{-1}$, respectively. The sensor resolution is found to be as low as $1.89 \times 10^{-6}$ RIU and $1.25 \times 10^{-6}$ RIU for the orthogonal modes. The lower peak birefringence method reveals a maximum wavelength sensitivity of 50,000 nm/RIU with a resolution of $2 \times 10^{-6}$ RIU. The sensitivity readings within the sensing range 1.42–1.47 are the highest among the reported sensors. The proposed sensor is indeed a suitable candidate to be practically implemented for analyte detections.

## CRediT authorship contribution statement

**M. Ifaz Ahmad Isti:** Conceptualization, Formal analysis, Investigation, Data curation, Writing - original draft. **Hriteshwar Talukder:** Formal analysis, Investigation, Data curation, Writing - original draft. **S.M. Riazul Islam:** Formal analysis, Investigation, Data curation, Funding acquisition, Writing - review & editing. **Samiha Nuzhat:** Formal analysis, Investigation, Data curation, Writing - review & editing. **A.S.M. Sanwar Hosen:** Formal analysis, Funding acquisition. **Gi Hwan Cho:** Formal analysis, Funding acquisition. **Shovasis Kumar Biswas:** Conceptualization, Formal analysis, Writing - review & editing.

## Declaration of Competing Interest

The authors declare that they have no known competing financial interests or personal relationships that could have appeared to influence the work reported in this paper.

## Acknowledgments

This work was supported in part by Independent University, Bangladesh (IUB), and in part by Sejong university through its faculty research program (20192021). This paper was also supported by research funds of Jeonbuk National University in 2020.

## References

[1] Fang S, Lee HJ, Wark AW, Corn RM. Attomole microarray detection of MicroRNAs by nanoparticle-amplified SPR imaging measurements of surface polyadenylation reactions. J Am Chem Soc 2006;128(43):14044–6.
[2] Stemmler I, Brecht A, Gauglitz G. Compact surface plasmon resonance-transducers with spectral readout for biosensing applications. Sensors Actuators, B Chem. 1999;54(1):98–105.
[3] Nooke A, et al. On the application of gold based SPR sensors for the detection of hazardous gases. Sensors Actuators, B Chem. 2010;149(1):194–8.
[4] Homola J. Present and future of surface plasmon resonance biosensors. Anal Bioanal Chem 2003;377(3):528–39.
[5] Hameed MFO, Obayya S. Comput Photon Sensors 2019.
[6] Talukder H, Isti MIA, Nuzhat S, Biswas SK. Ultra-high negative dispersion based single mode highly nonlinear bored core photonic crystal fiber (HNL-BCPCF): design and numerical analysis. Braz J Phys 2020;50(3):263–71.
[7] Ritchie RH. Plasma losses by fast electrons in thin films. Phys Rev 1956;106 N.5(5):8.
[8] Zenneck J. Über die Fortpflanzung ebener elektromagnetischer Wellen längs einer ebenen Leiterfläche und ihre Beziehung zur drahtlosen Telegraphie. Ann Phys 1907;328(10):846–66.
[9] Kretschmann E, Raether H. Radiative decay of non-radiative surface plasmons by light. Z. Naturforsch 1968;23(November):2135.
[10] Otto A. Excitation of nonradiative surface plasma waves in silver by the method of frustrated total reflection. Zeitschrift für Phys. 1968;216(4):398–410.
[11] Haque E, Anwar Hossain M, Namihira Y, Ahmed F. Microchannel-based plasmonic refractive index sensor for low refractive index detection. Appl Opt 2019;58(6):1547.
[12] Johnson PB, Christy RW. Optical Constant of the Nobel Metals. Phys. L Re View B 1972;6(12):4370–9.
[13] Fan Z, Li S, Liu Q, An G, Chen H, Li J, et al. High sensitivity of refractive index sensor based on analyte-filled photonic crystal fiber with surface plasmon resonance. IEEE Photon J 2015;7(3):1–9.
[14] Rifat A, Mahdiraji GA, Sua Y, Shee Y, Ahmed R, Chow DM, et al. Surface plasmon resonance photonic crystal fiber biosensor: A practical sensing approach. IEEE Photon Technol Lett 2015;27(15):1628–31.
[15] Pathak AK, Singh VK, Ghosh S, Rahman BMA. Investigation of a SPR based refractive index sensor using a single mode fiber with a large D shaped microfluidic channel. OSA Contin 2019;2(11):3008.
[16] Liu C, Su W, Wang F, Li X, Liu Q, Mu H, et al. Birefringent PCF-based SPR sensor for a broad range of low refractive index detection. IEEE Photonics Technol Lett 2018;30(16):1471–4.
[17] Sharma AK, Jha R, Gupta BD. Fiber-optic sensors based on surface plasmon resonance: a comprehensive review. IEEE Sens J Aug. 2007;7(8):1118–29.
[18] F. Haider, R. A. Aoni, R. Ahmed, S. Islam, and A. E. Miroshnichenko, Propagation controlled photonic crystal fiber based plasmonic sensor via scaled-down approach, vol. 1748, no. c, pp. 1–9, 2018.
[19] Han J, Su W, Liu C, Wang F, Xu C, Liu Q, et al. Asymmetrical photonic crystal fiber based on the surface plasmon resonance sensor and analysis by the lower-birefringence peak method. Optik 2019;189(May):121–9.
[20] Doron-mor I, Barkay Z, Filip-granit N, Vaskevich A, Rubinstein I. Ultrathin gold

island films on silanized glass. Morphol Optical Propert 2004;24:3476–83.
[21] A. H. A. R. Ifat, F. I. Haider, R. A. A. Hmed, G. H. A. M. M. Ahdiraji, F. R. M. A. A. Dikan, and A. N. E. M. Iroshnichenko, "Highly sensitive selectively coated photonic crystal fiber-based plasmonic sensor," vol. 43, no. 4, pp. 891–894, 2018.
[22] L. Li, G. Wylangowski, D. N. Payne, and R. Birch, "Broadband metal/glass single-mode fibre polarisers," vol. 22, no. 19, pp. 1020–1022, 1986.
[23] Weng, L. Pei, J. Wang, T. Ning and J. Li "High sensitivity D -shaped hole fiber temperature sensor based on surface plasmon resonance with liquid filling," vol. 5, no. 2, pp. 103–107, 2017.
[24] M. Al Mahfuz, A. Hossain, E. Haque, and N. H. Hai, "Dual-Core Photonic Crystal Fiber-Based Plasmonic RI Sensor in the Visible to Near-IR Operating Band," no. March, 2020.
[25] Haynes CL, Van Duyne RP. Nanosphere lithography: a versatile nanofabrication tool for studies of size-dependent nanoparticle optics. J Phys Chem B Jun. 2001;105(24):5599–611.
[26] Mishra AK, Mishra SK, Gupta BD. SPR based fiber optic sensor for refractive index sensing with enhanced detection accuracy and figure of merit in visible region. Opt Commun 2015;344:86–91.
[27] M. Al Mahfuz, M. R. Hasan, M. R. Momota, A. Masud, and S. Akter, "Asymmetrical photonic crystal fiber based plasmonic sensor using the lower birefringence peak method," OSA Continuum, vol. 2, no. 5, 2019.
[28] Rifat AA, Ahmed R, Mahdiraji GA, Adikan FRM. Highly sensitive D-shaped photonic crystal fiber-based plasmonic biosensor in visible to near-IR. IEEE Sens J 2017;17(9):2776–83.
[29] Chakma S, Khalek MA, Paul BK, Ahmed K, Hasan MR, Bahar AN. Gold-coated photonic crystal fiber biosensor based on surface plasmon resonance: Design and analysis. Sens. Bio-Sensing Res. 2018;18:7–12.
[30] Wu J, Li S, Wang X, Shi M, Feng X, Liu Y. Ultrahigh sensitivity refractive index sensor of a D-shaped PCF based on surface plasmon resonance. Appl Opt 2018;57(15):4002.
[31] Liu C, Yang L, Lu X, Liu Q, Wang F, Lv J, et al. Mid-infrared surface plasmon resonance sensor based on photonic crystal fibers. Opt Express 2017;25(13):14227–37.
[32] Haque E, Hossain MA, Ahmed F, Namihira Y. Surface Plasmon Resonance Sensor Based on Modified D-Shaped Photonic Crystal Fiber for Wider Range of Refractive Index Detection. IEEE Sens J 2018;18(20):8287–93.
[33] Islam MS, Cordeiro CM, Sultana J, Aoni RA, Feng S, Ahmed R, et al. A Hi-Bi Ultra-Sensitive Surface Plasmon Resonance Fiber Sensor. IEEE Access 2019;7(6):79085–94.
[34] Han H, Hou D, Zhao L, Luan N, Song L, Liu Z, et al. A large detection-range plasmonic sensor based on an h-shaped photonic crystal fiber. Sensors (Switzerland) 2020;20(4):1–8.
[35] Sakib MN, Islam SR, Mahendiran T, Abdulrazak LF, Islam MS, Mehedi IM, et al. Numerical study of circularly slotted highly sensitive plasmonic biosensor: A novel approach. Results Phys 2020;17:103130.
[36] Qiu G, Gai Z, Tao Y, Schmitt J, Kullak-Ublick GA, Wang J. Dual-functional plasmonic photothermal biosensors for highly accurate severe acute respiratory syndrome coronavirus 2 detection. ACS Nano 2020;14(5):5268–77.
[37] Anker JN, Hall WP, Lyandres O, Shah NC, Zhao J, van Duyne RP. Biosensing with plasmonic nanosensors. "Nanosci Technol 2009;557(5):308–19. Co-Published with Macmillan Publishers Ltd, UK.
[38] Samoc A. Dispersion of refractive properties of solvents: Chloroform, toluene, benzene, and carbon disulfide in ultraviolet, visible, and near-infrared. J Appl Phys 2003;94(9):6167–74.
[39] S. C. Tjin, "Bimetallic Silver – Gold Film Waveguide Surface Plasmon Resonance Sensor," no. February, pp. 229–240, 2007.
[40] Weng S, Pei L, Wang J, Ning T, Li J. High sensitivity D-shaped hole fiber temperature sensor based on surface plasmon resonance with liquid filling. Photonics Res 2017;5(2):103.
[41] Momtaj M, Hassan W, Amiri IS. "Numerical Study of Circularly Slotted Highly Sensitive Plasmonic Biosensor. A Novel" 2020.